INTERNATIONAL JOURNAL OF CLIMATOLOGY
Int. J. Climatol. **33**: 3073–3082 (2013)
Published online 15 December 2012 in Wiley Online Library
(wileyonlinelibrary.com) DOI: 10.1002/joc.3631

RMetS
Royal Meteorological Society

Short Communication

Tropopause level Rossby wave breaking in the Northern Hemisphere: a feature-based validation of the ECHAM5-HAM climate model

A. Béguin,[a†] O. Martius,[a,b*] M. Sprenger,[a] P. Spichtinger,[a,c] D. Folini[a] and H. Wernli[a]

[a] *Institute for Atmospheric and Climate Science, ETH Zurich, Zurich, Switzerland*
[b] *Oeschger Centre for Climate Change Research and Institute of Geography, University of Bern, Bern, Switzerland*
[c] *Institute for Atmospheric Physics, Johannes Gutenberg University Mainz, Mainz, Germany*

ABSTRACT: Breaking synoptic-scale Rossby waves (RWB) at the tropopause level are central to the daily weather evolution in the extratropics and the subtropics. RWB leads to pronounced meridional transport of heat, moisture, momentum, and chemical constituents. RWB events are manifest as elongated and narrow structures in the tropopause-level potential vorticity (PV) field. A feature-based validation approach is used to assess the representation of Northern Hemisphere RWB in present-day climate simulations carried out with the ECHAM5-HAM climate model at three different resolutions (T42L19, T63L31, and T106L31) against the ERA-40 reanalysis data set. An objective identification algorithm extracts RWB events from the isentropic PV field and allows quantifying the frequency of occurrence of RWB. The biases in the frequency of RWB are then compared to biases in the time mean tropopause-level jet wind speeds. The ECHAM5-HAM model captures the location of the RWB frequency maxima in the Northern Hemisphere at all three resolutions. However, at coarse resolution (T42L19) the overall frequency of RWB, i.e. the frequency averaged over all seasons and the entire hemisphere, is underestimated by 28%.The higher-resolution simulations capture the overall frequency of RWB much better, with a minor difference between T63L31 and T106L31 (frequency errors of −3.5 and 6%, respectively). The number of large-size RWB events is significantly underestimated by the T42L19 experiment and well represented in the T106L31 simulation. On the local scale, however, significant differences to ERA-40 are found in the higher-resolution simulations. These differences are regionally confined and vary with the season. The most striking difference between T106L31 and ERA-40 is that ECHAM5-HAM overestimates the frequency of RWB in the subtropical Atlantic in all seasons except for spring. This bias maximum is accompanied by an equatorward extension of the subtropical westerlies.

KEY WORDS climate model validation; Rossby wave breaking; potential vorticity; ECHAM5; ECHAM5-HAM; model resolution; jet streams

Received 8 September 2011; Revised 11 October 2012; Accepted 8 November 2012

1. Introduction

The validation of climate models is frequently based upon the comparison of model time-mean fields with reference climatologies. This approach does not allow assessing how well a specific synoptic-scale weather feature is represented in the model. However, the correct spatial and temporal distribution of these synoptic-scale flow structures in climate model simulations is crucial for a correct representation of climatological features (e.g. Palmer *et al.* 2008). Therefore, model validations focusing on specific weather features are important. Examples of feature-based validations of climate models include assessments of the frequency of blockings (e.g. D'Andrea *et al.* 1998; Sillmann and Croci-Maspoli, 2009; Matsueda *et al.* 2010), extra-tropical cyclones (e.g. Jung *et al.* 2006; Bengtsson *et al.* 2009), storm tracks (e.g. Ulbrich *et al.* 2008), and Rossby waves (Lucarini *et al.* 2007). In this study, we focus on the validation of the frequency and location of the occurrence of synoptic-scale Rossby wave breaking (RWB) at tropopause level.

Synoptic-scale RWB is a nonlinear process that can be a key trigger for high-impact weather events. It is characterized by the formation of meridionally elongated, zonally narrow intrusions of stratospheric high potential vorticity (PV) air into the troposphere (Appenzeller and Davies, 1992). These structures with anomalously high PV (compared to a PV climatology) can exert a profound far-field impact on the flow throughout the troposphere (Hoskins *et al.* 1985). In many cases, these narrow filaments break up, into so-called upper-level cut-off lows (e.g. Nieto *et al.* 2008), and thus represent an

* Correspondence to: O. Martius, Institute of Geography, University of Bern, Bern, Switzerland. e-mail: Olivia.martius@giub.unibe.ch

† Current address: Department of Applied Environmental Science (ITM), Stockholm University, Stockholm, Sweden.

irreversible deformation of PV contours. Both their far-field effect and the induced irreversible mixing underline the dynamical relevance of these structures.

RWB plays a central role in the daily weather evolution in the extra-tropics and has been observed to trigger heavy precipitation events in the extra-tropics. The cyclonic flow field that accompanies the breaking wave ensures the transport of large amounts of moisture toward the precipitation areas (e.g. Massacand *et al.* 1998; Martius *et al.* 2006; Roberge *et al.* 2009). In the subtropics and tropics, the breaking wave destabilizes the atmosphere (Funatsu and Waugh, 2008), which is of central importance for the triggering of heavy precipitation events in Africa (e.g. Knippertz, 2007) and the spawning of tropical cyclones (e.g. Davis and Bosart, 2003). Over 40% of all hurricanes are initiated by an upper-level baroclinic disturbance (McTaggart-Cowan *et al.* 2008).

On intra-seasonal time-scales, RWB events force major patterns of large-scale low-frequency variability in both hemispheres such as the North Atlantic Oscillation (NAO) (e.g. Benedict *et al.* 2004; Martius *et al.* 2007; Rivière and Orlanski, 2007), the Pacific North American pattern (Franzke *et al.* 2011), and the southern annular mode (Berrisford *et al.* 2007).

From a theoretical point of view, there are two canonical life-cycles of baroclinic waves that can lead to cyclonic (north-west to south-east elongation, LC2-type) or anticyclonic (south-west to north-east elongation, LC1-type) RWB, respectively (Davies *et al.* 1991; Thorncroft *et al.* 1993). The associated momentum fluxes are directed northwards for the cyclonic life-cycle resulting in a local northward shift and acceleration of the jet. Momentum fluxes are directed southwards for the anticyclonic life-cycle leading to a southward shift and local acceleration of the jet. The link between RWB life-cycles and the jets is, however, more involved. A more northerly (southerly) latitudinal location of the jets results in a preference for anticyclonic (cyclonic) life-cycles (Rivière, 2009) and consequently in a positive feedback that ensures persistence of the jet in a certain latitudinal position, bridging the time-scales to low-frequency patterns of variability (e.g. Gerber and Vallis, 2007; Rivière *et al.*2010; Rivière 2011).

RWB is also highly relevant for the vertical and horizontal distribution of trace gases in the tropopause-region due to the enhanced frequency of stratosphere–troposphere exchange in their vicinity (Sprenger *et al.* 2007) and the meridional redistribution of air masses with high and low ozone concentrations (Hood *et al.* 1999). Just below the tropopause, RWB can also lead to the formation of cirrus clouds (Eixmann *et al.* 2010), which is relevant, for instance, for the radiative energy budget in the tropopause region.

In this study, a detailed validation of the characteristics (frequency, location, and size) of RWB in the Northern Hemisphere in the ECHAM5-HAM climate model is presented for three different model resolutions. A resolution dependent validation is important because previous studies show that the model resolution is relevant for the representation of synoptic-scale features such as intense surface cyclones (Jung *et al.* 2006; Bengtsson *et al.* 2006). The focus on the ECHAM5-HAM model is motivated by the fact that this model is among the best global models concerning the representation of extratropical synoptic-scale flow features in present-day climate conditions (van Ulden and van Oldenborgh, 2006). In the next section, a brief description of the climate model and the RWB identification procedure is given, followed by a presentation of the main results in Section 3. Section 4 discusses the limitations of our approach, the dynamical ramifications of our findings, and the implications for ECHAM5-HAM climate simulations.

2. Data and methods

Three 44-year simulations of present-day climate conditions (1958–2001) with the ECHAM5-HAM global circulation model (Stier *et al.* 2005; Roeckner *et al.* 2006; Lohmann *et al.*2007) form the basis of this analysis. The runs differ in their horizontal and vertical resolution. Horizontally, spectral truncations at wave numbers 42, 63 and 106 are used. Depending on the horizontal resolution, 19 or 31 vertical levels are used (T42L19, T63L31, and T106L31). The spectral truncations roughly correspond to regular grids with resolutions of 2.8° (T42), 1.875° (T63), and 1.125° (T106). Model output is available 6-hourly for the T106, 12-hourly for the T63, and daily for the T42 simulation. Only 12-hourly output from the T106 simulation will be used for our analysis. All other aspects of the model setup are identical in the three simulations, including the model top at 10 hPa.

The vertical resolution of the T42 run (L19) is lower than that of the T63 and the T106 runs (L31) and this could affect the tropopause level flow. In terms of the zonal mean flow, however, Roeckner et al. (2006) found little differences in the Northern Hemisphere during the DJF season between T42L19 and T42L31 simulations performed with the ECHAM5-HAM model. They suggested that increasing the vertical resolution from 19 to 31 levels is only beneficial at horizontal resolutions above T63, based on a comparison of root-mean-square errors of selected fields to ERA-40.

The following external forcings have been applied for our simulations: (1) annual aerosol emission inventories obtained from the Japanese National Institute for Environmental Studies (NIES) were used in the Hamburg Aerosol Module (HAM) (Stier *et al.* 2005), (2) the ENSEMBLES sea-surface temperature and sea ice data set obtained from a coupled run of the HADCM3 model (Murphy *et al.* 2007) was used for the lower boundary condition, and (3) observation-based data by Solanki and Krivova (2003) was used for the radiative forcing.

The ERA-40 reanalysis data set by the European Center for Medium-Range Weather Forecasts (Uppala *et al.* 2005) is used as benchmark to assess the RWB

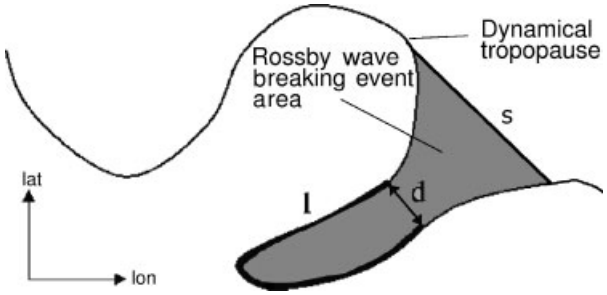

Figure 1. Schematic depiction of the RWB detection algorithm. Modified from Wernli and Sprenger (2007).

performance of ECHAM5-HAM. This data set covers the period 1958–2001 and has a 6-hourly temporal resolution. The instantaneous wind and temperature fields have been interpolated from T159 to a regular grid with 1° horizontal resolution.

For every data set and every time step, PV and wind speed have been calculated on model levels and interpolated onto isentropic surfaces between 310 and 350 K (every 10 K). We analyze RWB on several isentropic surfaces because they intersect the dynamical tropopause (2 PVU contour, 1 PVU = 10^{-6} K s^{-1} kg^{-1} m^2) at different latitudes, which allows identifying RWB in midlatitudes and the subtropics separately. We identify RWB events on these isentropic surfaces following the procedure outlined in Wernli and Sprenger (2007). In a first step, the 2-PVU contour is identified as a spherical polygon on an isentropic surface. In a second step, RWB structures are detected as elongated filaments along this contour using the criteria schematically shown in Figure 1. RWB is detected if stratospheric air masses are enclosed by a contour segment (with length l) that is longer than 2000 km and has a great circle distance (d) of less than 1500 km between the two end points of the segment. Finally, different from the method used by Wernli and Sprenger (2007), the area of the RWB event (i.e., the area enclosed by the contour segment) is extended into the stratosphere from its most narrow constriction until the line separating the RWB from the main body of stratospheric air (s) has a length of 2000 km on the considered isentrope.

The result is a binary field indicating the presence or absence of RWB at each grid point, for every isentropic level and for each time step. Time averaging of these fields for each season (DJF, MAM, JJA, SON) yields seasonal frequency fields (displayed as percentage, i.e. multiplied by 100) for the occurrence of RWB. To allow for a compact visualization of the results the RWB information is vertically aggregated across the considered isentropic surfaces. At each time step, this new vertically aggregated binary field has a value of 1 at a certain grid point if a RWB event is detected on any of the considered isentropic levels (and a value of 0 otherwise). These fields are then again time averaged to produce seasonal frequency fields.

3. Results

3.1. Validation of vertically aggregated RWB frequencies and jet wind speeds

Figure 2 shows the occurrence frequency of the vertically aggregated RWB for all seasons in the ECHAM5-HAM simulations and in ERA-40. Also, the seasonal mean horizontal wind speed on 350 K in summer and on 330 K during the other seasons (red contours) and the hemispheric maximum seasonal mean jet wind speed (blue labels) are shown. The RWB frequency maxima are located in similar geographical locations in ERA-40 and in all model simulations, namely to the north and downstream of the seasonal mean jet streams in winter, spring, and fall and over the subtropical ocean basins and the Asian continent in summer. This is in agreement with earlier climatologies based on reanalysis data by Wernli and Sprenger (2007) and Martius *et al.*(2008). In winter, the wind maximum of the Pacific jet is underestimated by 4.5 m s^{-1} in the T42L19 run (Figure 2, first row). In spring, the jet stream maximum of the Pacific jet is overestimated by approximately 5 m s^{-1} in all model resolutions (Figure 2, second row). In summer, the jet is too strong in the Atlantic basin and too weak in the Pacific basin in the T42L19 run (Figure 2, third row). In fall, the jet maxima are reasonably well captured by the model.

Seasonal mean absolute differences of the aggregated RWB fields and the isentropic wind speeds between the ECHAM5-HAM model simulations and ERA-40 are shown in Figure 3. The wind differences are calculated for the same isentropic levels used in Figure 2. The positive and negative RWB frequency biases in the T42L19 experiment averaged over the entire Northern Hemisphere and over all seasons amount to an underestimation of the frequency by 28% compared to ERA-40. In contrast, the RWB frequency is much better represented in the T63L31 and T106L31 runs for which the hemispherically averaged biases amount to −3.5% in T63L31 and +6.0% in T106L31. The biases of the hemispherically and seasonally averaged horizontal wind speed indicate an overestimation of the winds by 4.8% (or 0.33 m s^{-1}) in the T42L19 experiment, by 10.4% (or 0.73 m s^{-1}) in the T63L31 experiment, and by 10.2% (0.7 m s^{-1}) in the T106L31 experiment.

Substantial regional differences exist between all model simulations and the ERA-40 RWB distribution. The spatial structure of the biases is similar for all three model resolutions. The RWB frequency is generally overestimated by ECHAM5-HAM in the subtropics (Figure 3), namely over the subtropical Atlantic (DJF, JJA, and SON), East Asia (JJA), and the subtropical Pacific (JJA and SON). The RWB frequency is generally underestimated in the extratropics (Figure 3). In the T42L19 simulations frequencies are underestimated in the entire Northern Hemisphere, the largest negative biases are found in JJA in the extratropics over Europe and the western Pacific (Figure 3(g)) and in SON over North America (Figure 3(k)). In the higher resolution simulations the negative biases are located over the Pacific

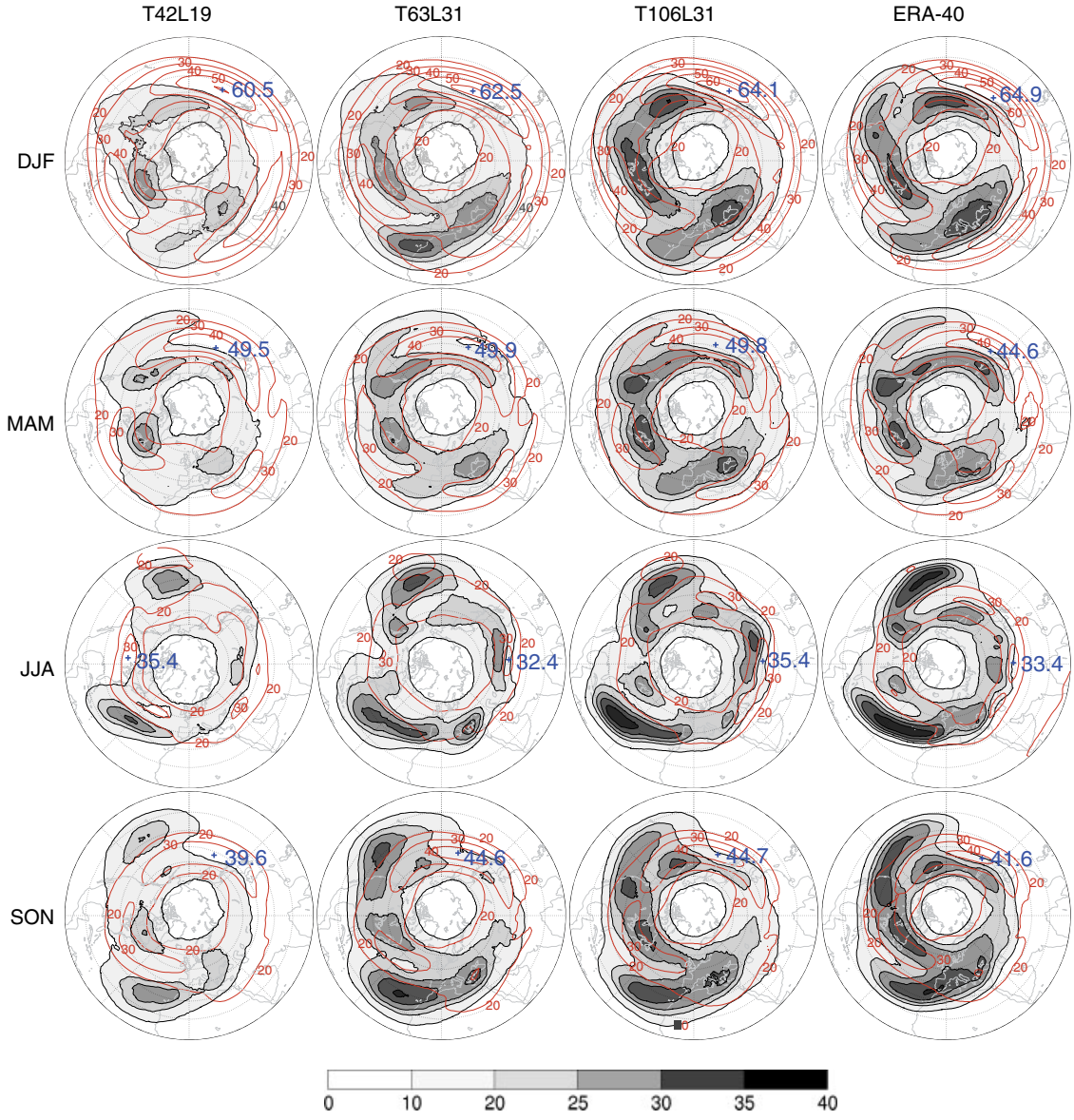

Figure 2. Vertically aggregated RWB frequency (grey shading) in the three ECHAM5-HAM simulations (from left to right: T42L19, T63L31, T106L31) and in the ERA-40 data set (rightmost column), mean wind velocity (red contours), and maximum of mean wind velocity (blue cross) for all seasons (from top to bottom: DJF, MAM, JJA, and SON). Wind velocities are shown on 330 K for DJF, MAM and SON, and on 350 K for JJA.

storm track (SON, DJF, MAM) and over Europe (JJA) (Figure 3, second and third column).

The biases in the number of RWB events go along with biases in the jet streams on the dynamically relevant isentropic surfaces. In winter, the jet is too strong and too zonal in the Atlantic sector in the models compared to ERA-40 (Figures 2 and 3, first row). The winter jet configuration over the North Atlantic in the ECHAM5-HAM model corresponds to a negative NAO phase while the North Atlantic flow in ERA-40 bears a stronger resemblance to a positive NAO jet configuration (Figure 2, first row). The biases are strongest in the T42L19 run and weakest in T106L31 (Figure 3). This jet bias has been previously observed for ECHAM4 (Pinto *et al.* 2006) and for ECHAM5 and has been linked to an underestimation of the blocking frequencies in ECHAM5 (Pinto *et al.* 2007). Rivière *et al.*(2010) find similar biases in the jet over the Atlantic for simulations of the pre-industrial climate in the CNRM-CM3.3 and the HadCM3 climate models. The jet biases are accompanied by an underestimation of anticyclonic RWB in the Atlantic basin. In spring, the overall biases are small with a slight overestimation of the jet wind speed in the models in the Pacific (Figure 3(d)–(f)).

In the tropics, a zone of stronger westerlies extends further equatorward in the models compared to ERA-40 (Figure 3). This is most pronounced during summer when the wind speed in the tropics is overestimated in the models both in the Atlantic and the Pacific basin (Figure 3, third row). In fall, winds are overestimated in all ECHAM5-HAM runs in the tropical Atlantic (Figure 3, fourth row).

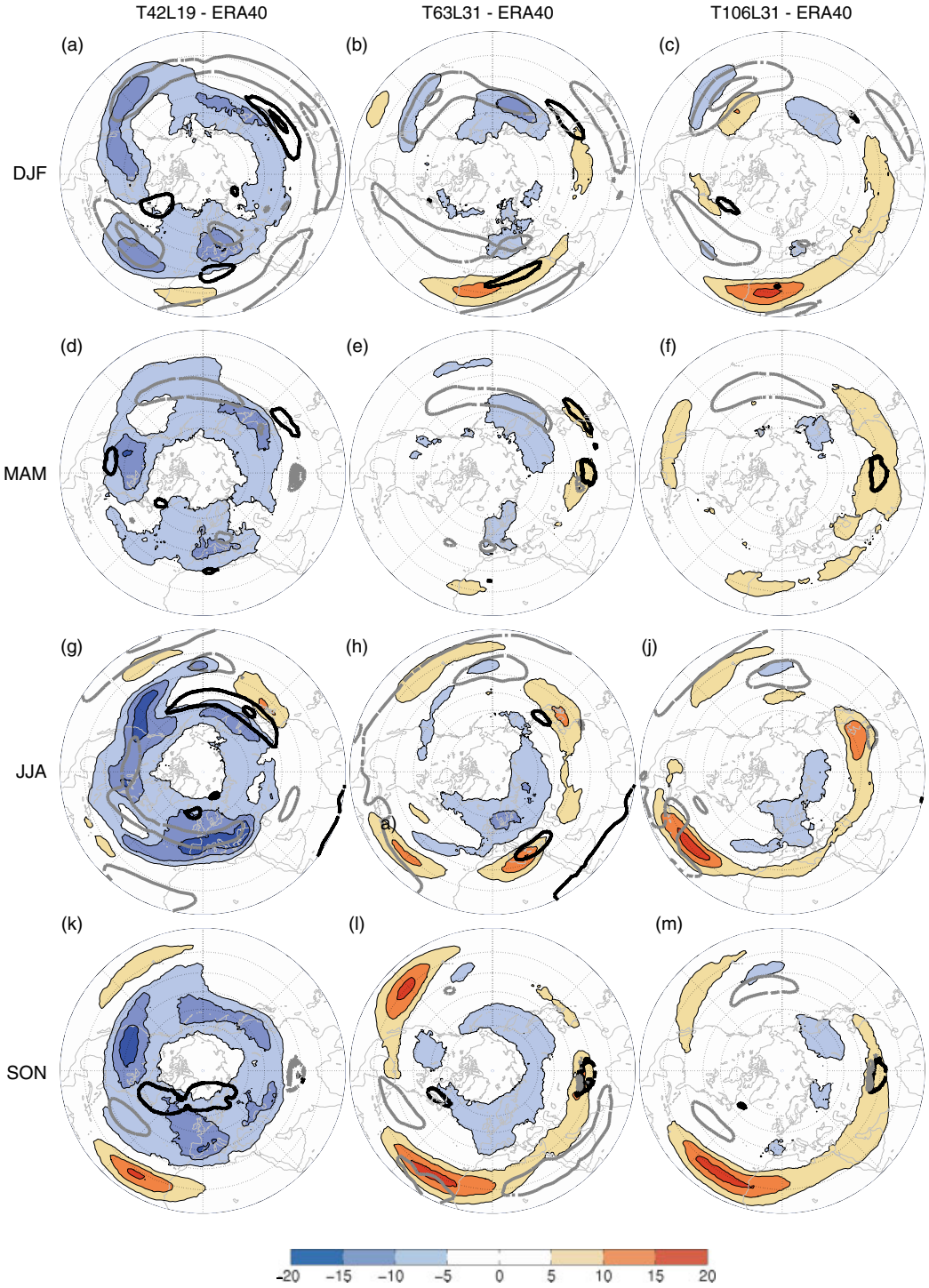

Figure 3. Difference in vertically aggregated RWB frequency (310, 330, and 350 K) between the ECHAM5-HAM simulation and ERA-40 during all seasons (from top to bottom: DJF, MAM, JJA, and SON). Contour lines indicate differences in wind speed when compared to ERA-40 (green: higher wind speed in ECHAM5, black: higher wind speed in ERA-40).

3.2. RWB frequencies and biases on individual isentropic surfaces

The isentropic levels intersecting the tropopause in the extratropics and the subtropics contribute complementary information to the overall picture and it is therefore useful to consider them separately. Different processes are relevant for the generation of RWB in the extratropics and the subtropics. Extratropical RWB events occurring on the 310 K level in winter and on the 330 K level in summer usually constitute the final stage in the life-cycle of a midlatitude baroclinic wave. They are closely linked to the extratropical surface weather evolution and typically accompanied by surface cyclones (e.g. Davies *et al.* 1991). The formation of subtropical RWB events on the 350 K level, on the other hand, is closely linked to

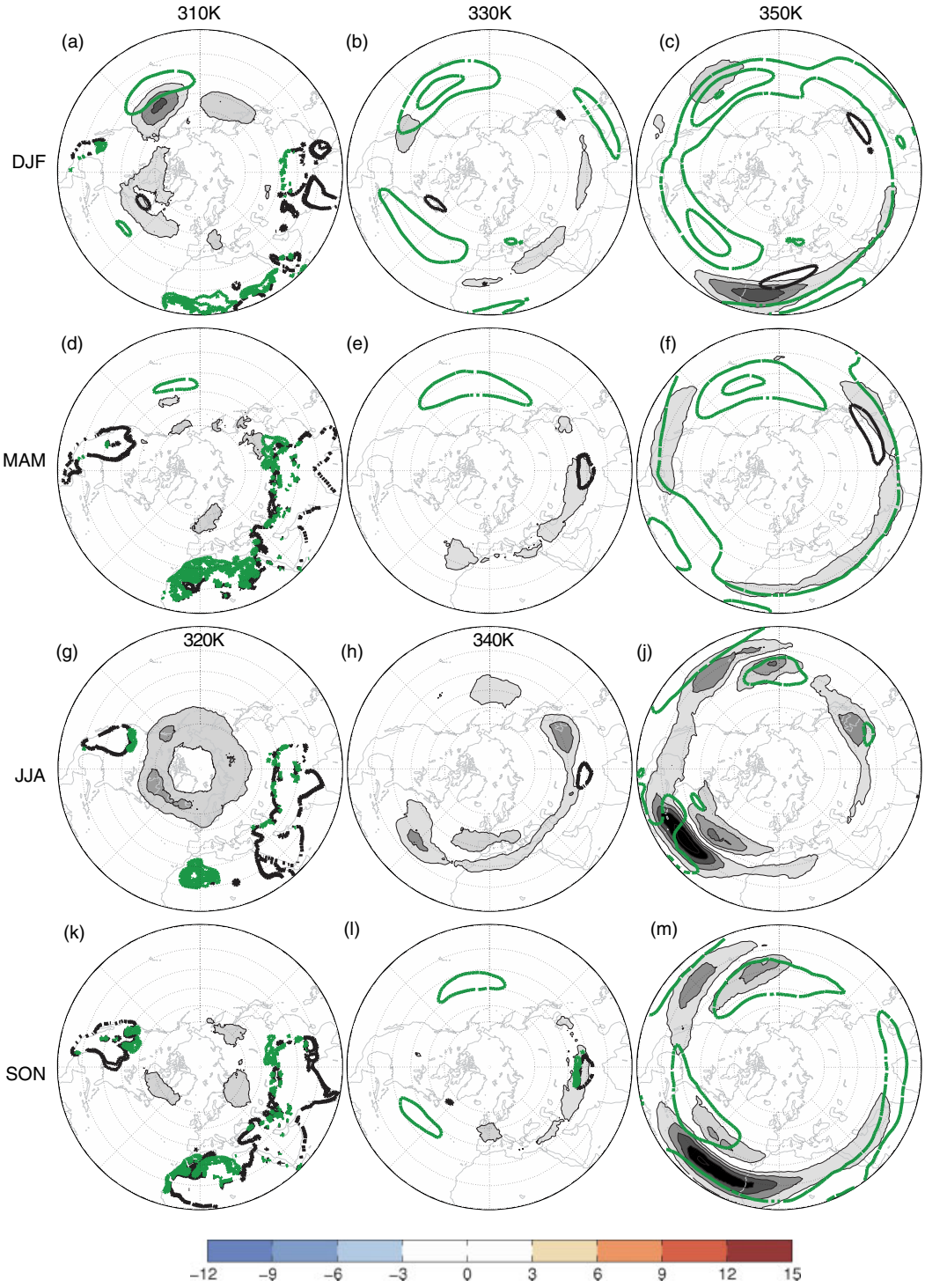

Figure 4. Difference in RWB frequency between the T106L31 simulation and ERA-40 on three isentropic levels (from left to right: 310, 330, and 350 K; 320 and 340 K for JJA) during all seasons (from top to bottom: DJF, MAM, JJA, and SON). Contour lines indicate differences in wind speed (green: higher wind speed in ECHAM5, black: higher wind speed in ERA-40).

the planetary-scale subtropical anticyclones (e.g. Postel and Hitchman, 1999). These RWB events are typically located on the downshear flank of the subtropical anticyclones. Some of these RWB events form through passive southward advection of stratospheric high PV air by the subtropical anticyclone and these RWB events are not linked to surface cyclones. However, they can be strongly influenced by tropical convection via the convectively induced strengthening of the subtropical anticyclones and the subsequent formation of RWB events (e.g. Randel and Park, 2006).

Figure 4 shows the difference in the RWB frequency in the T106L31 simulation with respect to ERA-40 on three isentropes highlighting processes along the extratropical tropopause (320 K in summer, 310 K in the other seasons), the subtropical tropopause (350 K) and

on an intermediate level (340 K in summer, 330 K in the other seasons). The contour lines show differences in isentropic wind speed.

During winter, the main differences to ERA-40 along the extratropical tropopause (i.e. on 310 K) have the form of an east–west dipole located in the Pacific basin (Figure 4(a)). During this season, the T106L31 RWB frequency maximum in the Pacific is zonally confined to the western Pacific (Figure 2), resulting in the dipole structure over the Pacific (Figure 4(a)). On 350 K the modelled frequency of RWB is higher than in ERA-40 in the subtropical Atlantic and lower than in ERA-40 in the subtropical western Pacific (Figure 4(c)). The jet wind speed is overestimated in the western Pacific on all levels. Note that the positive wind bias is located south of the positive RWB bias and to the north of the negative RWB bias in the Pacific (Figure 4, first row). In the Atlantic the previously discussed jet bias pattern, resembling a negative NAO phase, is again evident.

In spring, the RWB frequency biases to ERA-40 are small on all levels. A band of positive RWB frequency biases in the T106L31 experiment is found near the southern edge of the subtropical jet over Africa, Asia, and Central America (Figure 4(f)). A band of positive wind speed differences is located in the tropics south of the positive RWB frequency bias areas (Figure 4(f)).

In summer, ECHAM5-HAM underestimates the RWB frequency in the extratropics (i.e. on the 320 K) by at least 50% in most locations (Figure 4(g)). On the 350 K level, there are large positive biases of the RWB frequency over the subtropical Atlantic, the subtropical Pacific, and eastern Asia, even larger than the one observed during DJF (Figure 4(j)). Over the Atlantic and the Pacific, these overestimates go along with a negative bias further north, indicating a strong southward shift of the simulated RWB events. The ECHAM5-HAM wind velocities show a positive bias of about 5 m s^{-1} over the tropical oceans (Figure 4(j)).

During fall, there is an overestimation of RWB frequency on the 350 K level in the tropical Atlantic and an underestimation of the RWB frequency to the north in the subtropics, similar to the results for JJA (Figure 4(m)). Locally, the biases amount to 50% of the absolute frequency. A similar structure is present in the Pacific.

In summary, it can be stated that the largest frequency biases are found in the subtropical Atlantic. While relatively small-scale errors, although relevant for daily weather evolution, dominate on the lower levels, large-scale error patterns are seen on the 350 K level for all seasons.

4. Discussion

4.1. Sensitivity of results to the detection method

Before summarizing and discussing the potential implications of our model validation, we briefly recall some characteristics of the RWB frequency measure, which might have influenced our findings. Our RWB frequency measure depends on the number, the spatial scale and the lifetime of individual RWB events. The information given in Figure 2 does not reveal the relative importance of these three factors for the overall patterns. Here, we present additional evaluations concerning the areal extent of each RWB event, and the effects of the vertical position of the dynamical tropopause and the isentropic surfaces on our results.

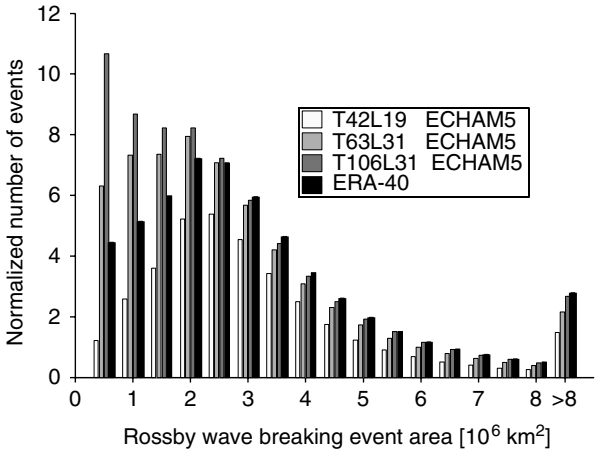

Figure 5. Size distribution of the individual RWB events for the three ECHAM5-HAM simulations and the ERA-40 dataset. All seasons and vertical levels (isentropes) are considered. Only daily output was available from the T42L19 simulation (12-hourly for T63L31 and T106L31), therefore the number of events found were divided by the number of analyzed output time steps and are hence 'normalized'. For each resolution, the resulting number reflects the average number of RWB of one size class found on all six isentropes for one time step.

The size distribution of all RWB events is shown in Figure 5 for the three ECHAM5-HAM simulations and the ERA-40 reanalysis. The number of large RWB events (events with an area larger than 3×10^6 km^2) increases when the model resolution is increased. In the T42L19 experiment the number of these events is underestimated by 39% compared to ERA-40. The substantial underestimation of the overall RWB frequency in the T42 simulation is hence mainly due to an underestimation of the number of large RWB structures. A tracking analysis would be required to estimate the lifetime of individual events and thus to determine whether the T42 simulations mainly underestimate the number of large RWB events or their lifetime. At higher resolution, the underestimation of large RWB events is less dramatic (15% in T63L31, 3% in T106L31). In contrast, the higher-resolution simulations overestimate the frequency of RWB events with areas smaller than 2×10^6 km^2. These small-scale RWB structures occur mainly on the uppermost level considered and are therefore (and because of their small scale) of minor dynamical importance for the surface weather.

Since the RWB detection algorithm analyses the curvature of the dynamical tropopause on an isentropic surface, the outcome depends on the respective vertical position of these surfaces. An upward bias in the vertical position of the isentrope would lead to a northward latitudinal shift in the RWB frequency pattern when keeping

the vertical position of the dynamical tropopause fixed. To quantify this effect, the bias of the zonal-mean latitudinal position of the dynamical tropopause is compared with the mean latitudinal shift in the RWB location. The zonal-mean position of the tropopause is approximated by the zonal average of the latitude where the dynamical tropopause intersects the 315, 330, and 350 K isentropic surfaces and subsequent averaging of these three values. The mean latitudinal bias in the RWB frequency was calculated by subtracting the latitude of the zonal-mean RWB frequency maximum in ECHAM5-HAM from the corresponding ERA-40 latitude for each level, season and model resolution. In the last step the values for the individual isentropes are averaged to obtain one seasonal estimate of latitudinal RWB location bias.

In the low-resolution model (T42L19), the zonal mean latitudinal shift of the tropopause amounts to an equatorward displacement of about 2.7° during winter. This equatorward bias in tropopause location is larger than the latitudinal bias in RWB location and corresponds to a shift by less than one grid-point. Similar shifts are found for the other seasons, with the exception of JJA, where the RWB latitudinal bias is larger than the bias in tropopause location. The higher-resolution model versions capture the latitudinal location of the zonally averaged tropopause better, and like in the low-resolution model the biases are smaller than the latitudinal distance between two model grid-points. The corresponding mean latitudinal biases of the RWB breaking events are considerably larger, about 0–2° in the T42L19 run, and 2–4° in the T63L31 and the T106L31 runs, respectively. These biases are therefore the result of the model dynamics, which places the RWB events in different places than observed in ERA-40, and do not merely reflect errors in the tropopause location.

4.2. Dynamical implications and interpretation

The dynamical implications of biases in RWB frequency depend on their geographical location. RWB in the extratropics is often located within and downstream of the storm track area (e.g. RWB on 310 K in winter), where it strongly affects the surface weather evolution. It is further closely linked to the location and strength of the extratropical jet stream and thereby to low frequency patterns of variability in a complex, nonlinear way (e.g. Rivière and Orlanski, 2007; Rivière, 2009; Rivière *et al.*2010). An example from the T106L31 simulation is the RWB bias pattern in the Pacific basin on 310 K in winter (Figure 4, first panel), which is accompanied by an eastward and southward extension of the jet south of the positive RWB bias (see Figures 1 and 3). This eastward extension can be explained by the differences in the wave-breaking pattern. The breaking waves over the eastern Pacific are mainly southeast-northwest oriented LC2-type (Martius *et al.* 2007), and the momentum transport associated with this type of RWB accelerates the jet to the south of the RWB maximum resulting in an eastward extension of the jet. The decrease in subtropical RWB on the 350 K isentrope in the same longitudinal band, on the other hand, could be the result of the zonally extended and slightly more southward extension of the jet (Figure 4). In the North Atlantic, a similar positive bias in extratropical LC2-type RWB in DJF is associated with a positive wind bias in the western and central Atlantic (Figure 3(c)).

The differences in the RWB over the subtropical Atlantic during winter (Figures 3 and 4, first row) are linked to differences in the jet location and strength over the Atlantic basin. RWB events in the subtropics are mainly northeast-southwest oriented LC1-type events and coincide with double jet configurations (Martius *et al.* 2007). An overestimation of the frequency of this type of RWB goes along with an underestimation of the jet strength at the latitude of the RWB maximum and an overestimation of the jet strength to the north and to the south of it. In accordance the subtropical jet over Africa is weaker in the T106L31 simulation but the (westerly) winds over subtropical and equatorial eastern Atlantic are stronger than in ERA-40 (Figure 4(c)), indicating a southwards shift of the zero westerly wind line. Again a positive feedback mechanism could enhance this bias pattern: a southwards shift of the zero westerly wind line (a so-called westerly duct) allows the waves to propagate further south before they break and the breaking waves in return strengthen the westerly winds along their southern flanks.

A bias in the frequency of RWB in the subtropics and tropics has also potentially relevant dynamical ramifications. The positive RWB bias over the subtropical central and western Atlantic in summer (see Figure 4(j)) is located in an area where RWB events have been observed to trigger the formation of hurricanes (Davis and Bosart, 2003). A misrepresentation of RWB in addition affects the cross-tropopause exchange of tracers both in the extratropics and the subtropics (Sprenger *et al.* 2007). The difference in the RWB frequency over the tropical Atlantic during summer and fall, for example, might affect the upper-tropospheric moisture budget (e.g. Waugh, 2005).

By looking into the processes that are the main sources of variability of RWB in specific geographical areas, we can speculate about potential causes for the errors found in the RWB patterns in the T63L31 and the T106L31 simulations. In winter, both the El Niño Southern Oscillation and the Madden Julian Oscillation significantly influence the RWB distribution and frequency in the extratropical and subtropical Pacific basin (Shapiro *et al.* 2001; Moore *et al.* 2010). The Asian summer monsoon directly influences the location and frequency of RWB over Asia and the eastern Pacific (Randel and Park, 2006, Martius *et al.* 2008). RWB structures in the tropics and subtropics are in general closely linked to the strength and position of the semipermanent subtropical high-pressure systems (Postel and Hitchman, 1999), which in turn depend on the correct representation of the monsoon systems (Rodwell and Hoskins, 2001). A misrepresentation of any of these

forcings would lead to errors in the frequency of RWB in the according season and geographical area.

In summary, we conclude that the spatial distribution of the RWB maxima is fairly well represented in all ECHAM5-HAM simulations. Compared to ERA-40, the hemispheric mean frequency is underestimated by approximately 28% in the T42L19 run, mainly due to an underestimation of the large RWB structures. In the T63L31 and T106L31 simulations the mean frequency error is small (−3.5 and 6%, respectively). Isentropically averaged wind speeds are overestimated in all three model simulations. The average bias taken over all four seasons in the T42 simulation is +4.8% (in absolute terms: $0.33\,\mathrm{m\,s^{-1}}$), and larger in the other simulations (T63: +10.4% or $0.74\,\mathrm{m\,s^{-1}}$, T106: +10.2% or $0.71\,\mathrm{m\,s^{-1}}$). Locally, significant differences in the RWB frequency between the T106L31 simulation and the ERA-40 data are present, which affect important characteristics of the time-mean flow. Based on our analysis, we suggest that ECHAM5-HAM simulations should be performed at resolutions of T63L31 or higher if resources allow.

Acknowledgements

This study was supported by NCCR Climate. ECHAM5-HAM simulations were performed at the Swiss National Supercomputing Center, CSCS Manno, within the framework of the ALPS project. This work was supported by a grant from the Swiss National Supercomputing Centre (CSCS) under project ID s235. The Center for Climate Systems Modeling (C2SM) at ETH Zurich is acknowledged for providing technical and scientific support. The authors thank Huw Davies, Christoph Schär, Ulrike Lohmann, Martin Wild, Hans Feichter, Erich Roeckner, and Philip Stier for support and valuable discussions and MeteoSwiss for providing access to the ERA-40 data. We thank one anonymous reviewer for the valuable feedback.

References

Appenzeller C, Davies HC. 1992. Structure of stratospheric intrusions into the troposphere. *Nature* **358**: 570–572.

Benedict JJ, Lee S, Feldstein SB. 2004. Synoptic view of the North Atlantic Oscillation. *Journal of the Atmospheric Sciences* **61**: 121–144.

Bengtsson L, Hodges KI, Roeckner E. 2006. Storm tracks and climate change. *Journal of Climate* **19**: 3518–3543.

Bengtsson L, Hodges KI, Keenlyside N. 2009. Will extratropical storms intensify in a warmer climate? *Journal of Climate* **22**: 2276–2301.

Berrisford P, Hoskins BJ, Tyrlis E. 2007. Blocking and Rossby wave breaking on the dynamical tropopause in the Southern Hemisphere. *Journal of the Atmospheric Sciences* **64**: 2881–2898.

D'Andrea F, Tibaldi S, Blackburn M, Boer G, Deque M, Dix MR, Dugas B, Ferranti L, Iwasaki T, Kitoh A, Pope V, Randall D, Roeckner E, Strauss D, Stern W, Van den Dool H, Williamson D. 1998. Northern Hemisphere atmospheric blocking as simulated by 15 atmospheric general circulation models in the period 1979–1988. *Climate Dynamics* **14**: 385–407.

Davies HC, Schär C, Wernli H. 1991. The palette of fronts and cyclones within a baroclinic wave development. *Journal of the Atmospheric Sciences* **48**: 1666–1689.

Davis CA, Bosart LF. 2003. Baroclinically induced tropical cyclogenesis. *Monthly Weather Review* **131**: 2730–2747.

Eixmann R, Peters DHW, Zuelicke C, Gerding M, Dörnbrack A. 2010. On the upper tropospheric formation and occurrence of high and thin cirrus clouds during anticyclonic poleward Rossby wave breaking events. *Tellus Series A: Dynamic Meteorology and Oceanography* **62**: 228–242. DOI: 10.1111/j.1600-0870.2010.00437.x.

Franzke C, Feldstein SB, Lee S. 2011. Synoptic analysis of the Pacific-North American teleconnection pattern. *Quarterly Journal of the Royal Meteorological Society* **137**: 329–346.

Funatsu BM, Waugh DW. 2008. Connections between potential vorticity intrusions and convection in the eastern tropical pacific. *Journal of the Atmospheric Sciences* **65**: 987–1002.

Gerber EP, Vallis GK. 2007. Eddy-zonal flow interactions and the persistence of the zonal index. *Journal of the Atmospheric Sciences* **64**: 3296–3311.

Hood L, Rossi S, Beulen M. 1999. Trends in lower stratospheric zonal winds, Rossby wave breaking behavior, and column ozone at northern midlatitudes. *Journal of Geophysical Research-Atmospheres* **104**: 24321–24339.

Hoskins BJ, McIntyre ME, Robertson AW. 1985. On the use and significance of isentropic potential vorticity maps. *Quarterly Journal of the Royal Meteorological Society* **111**: 877–946.

Jung T, Gulev SK, Rudeva I, Soloviov V. 2006. Sensitivity of extratropical cyclone characteristics to horizontal resolution in the ECMWF model. *Quarterly Journal of the Royal Meteorological Society* **132**: 1839–1857.

Knippertz P. 2007. Tropical-extratropical interactions related to upper-level troughs at low latitudes. *Dynamics of Atmospheres and Oceans* **43**: 36–62.

Lohmann U, Stier P, Hoose C, Ferrachat S, Kloster S, Roeckner E, Zhang J. 2007. Cloud microphysics and aerosol indirect effects in the global climate model ECHAM5-HAM. *Atmospheric Chemistry and Physics* **7**: 3425–3446.

Lucarini V, Calmanti S, Dell'Aquila A, Ruti PM, Speranza A. 2007. Intercomparison of the northern hemisphere winter mid-latitude atmospheric variability of the IPCC models. *Climate Dynamics* **28**: 829–848.

Martius O, Zenklusen E, Schwierz C, Davies HC. 2006. Episodes of Alpine heavy precipitation with an overlying elongated stratospheric intrusion: a climatology. *International Journal of Climatology* **26**: 1149–1164.

Martius O, Schwierz C, Davies HC. 2007. Breaking waves at the tropopause in the wintertime Northern Hemisphere: climatological analyses of the orientation and the theoretical LC1/2 classification. *Journal of the Atmospheric Sciences* **64**: 2576–2592.

Martius O, Schwierz C, Sprenger M. 2008. Dynamical tropopause variability and potential vorticity streamers in the northern hemisphere – a climatological analysis. *Advances in Atmospheric Sciences* **25**: 367–380.

Massacand AC, Wernli H, Davies HC. 1998. Heavy precipitation on the Alpine southside: an upper-level precursor. *Geophysical Research Letters* **25**: 1435–1438.

Matsueda M, Hirokazu E, Ryo M. 2010. Future change in Southern Hemisphere summertime and wintertime atmospheric blockings simulated using a 20-km-mesh AGCM. *Geophysical Research Letters* **37**: L02803. DOI: 10.1029/2009GL041758.

McTaggart-Cowan R, Deane GD, Bosart LF, Davis CA, Galarneau TJ. 2008. Climatology of tropical cyclogenesis in the North Atlantic (1948–2004). *Monthly Weather Review* **136**: 1284–1304.

Moore RW, Martius O, Spengler T. 2010. The Modulation of the Subtropical and Extratropical Atmosphere in the Pacific Basin in Response to the Madden–Julian Oscillation. *Monthly Weather Review* **138**: 2761–2779.

Murphy JM, Booth BBB, Collins M, Harris GR, Sexton DMH, Webb MJ. 2007. A methodology for probabilistic predictions of regional climate change from perturbed physics ensembles. *Philosophical Transactions of the Royal Society A: Mathematical, Physical and Engineering Sciences* **365**: 1993–2028.

Nieto R, Sprenger M, Wernli H, Trigo RM, Gimeno L. 2008. Identification and climatology of cut-off lows near the tropopause. *Annals of the New York Academy of Sciences* **1146**: 256–290. DOI: 10.1196/annals.1446.016

Palmer TN, Doblas-Reyes FJ, Weisheimer A, Rodwell MJ. 2008. Toward seamless prediction: calibration of climate change projections using seasonal forecasts. *Bulletin of the American Meteorological Society* **89**: 459–470.

Pinto JG, Spangehl T, Ulbrich U, Speth P. 2006. Assessment of winter cyclone activity in a transient ECHAM4-OPYC3 GHG experiment. *Meteorologische Zeitschrift* **15**: 279–291.

Pinto JG, Ulbrich U, Leckebusch GC, Spangehl T, Reyers M, Zacharias S. 2007. Changes in storm track and cyclone activity in three SRES ensemble experiments with the ECHAM5/MPI-OM1 GCM. *Climate Dynamics* **29**: 195–210.

Postel GA, Hitchman MH. 1999. A climatology of Rossby wave breaking along the subtropical tropopause. *Journal of the Atmospheric Sciences* **56**: 359–373.

Randel WJ, Park M. 2006. Deep convective influence on the Asian summer monsoon anticyclone and associated tracer variability observed with Atmospheric Infrared Sounder (AIRS). *Journal of Geophysical Research-Atmospheres* **111**: D12314. DOI: 10.1029/2005JD006490.

Rivière G. 2009. Effect of latitudinal variations in low-level baroclinicity on Eddy life cycles and upper-tropospheric wave-breaking processes. *Journal of the Atmospheric Sciences* **66**: 1569–1592.

Rivière G. 2011. A dynamical interpretation of the poleward shift of the jet streams in global warming scenarios. *Journal of the Atmospheric Sciences* **68**: 1253–1272.

Rivière G, Orlanski I. 2007. Characteristics of the Atlantic storm-track eddy activity and its relation with the North Atlantic Oscillation. *Journal of the Atmospheric Sciences* **64**: 241–266.

Rivière G, Laine A, Lapeyre G, Salas-Melia D, Kageyama M. 2010. Links between Rossby wave breaking and the North Atlantic Oscillation-Arctic Oscillation in present-day and the last glacial maximum climate simulations. *Journal of Climate* **23**: 2987–3008.

Roberge A, Gyakum JR, Atallah EH. 2009. Analysis of intense poleward water vapor transports into high latitudes of western North America. *Weather and Forecasting* **24**: 1732–1747.

Rodwell MJ, Hoskins BJ. 2001. Subtropical anticyclones and summer monsoons, *Journal of Climate* **14**: 3192–3211. DOI: 10.1175/1520-0442(2001)014.

Roeckner E, Brokopf R, Esch M, Giorgetta M, Hagemann S, Kornblueh L, Manzini E, Schlese U, Schulzweida U. 2006. Sensitivity of simulated climate to horizontal and vertical resolution in the ECHAM5 atmosphere model. *Journal of Climate* **19**: 3771–3791.

Shapiro MA, Wernli H, Bond NA, Langland R. 2001. The influence of the 1997–99 El Nino Southern Oscillation on extratropical baroclinic life cycles over the eastern North Pacific. *Quarterly Journal of the Royal Meteorological Society* **127**: 331–342.

Sillmann J, Croci-Maspoli M. 2009. Present and future atmospheric blocking and its impact on European mean and extreme climate. *Geophysical Research Letters* **36**: L10702. DOI: 10.1029/2009GL038259.

Solanki SK, Krivova NA. 2003. Can solar variability explain global warming since 1970? *Journal of Geophysical Research: Space Physics* **108**: 1200. DOI: 10.1029/2002JA009753.

Sprenger M, Wernli H, Bourqui M. 2007. Stratosphere-troposphere exchange and its relation to potential vorticity streamers and cutoffs near the extratropical tropopause. *Journal of the Atmospheric Sciences* **64**: 1587–1602. DOI: 10.1175/JAS3911.1.

Stier P, Feichter J, Kinne S, Kloster S, Vignati E, Wilson J, Ganzeveld L, Tegen I, Werner M, Balkanski Y, Schulz M, Boucher O, Minikin A, Petzold A. 2005. The aerosol-climate model ECHAM5-HAM. *Atmospheric Chemistry and Physics* **5**: 1125–1156.

Thorncroft CD, Hoskins BJ, McIntyre MF. 1993. Two Paradigms of baroclinic-wave life-cycle behaviour. *Quarterly Journal of the Royal Meteorological Society* **119**: 17–55.

Ulbrich U, Pinto JG, Kupfer H, Leckebusch GC, Spangehl T, Reyers M. 2008. Changing northern hemisphere storm tracks in an ensemble of IPCC climate change simulations. *Journal of Climate* **21**: 1669–1679.

van Ulden AP, van Oldenborgh GJ. 2006. Large-scale atmospheric circulation biases and changes in global climate model simulations and their importance for climate change in Central Europe. *Atmospheric Chemistry and Physics* **6**: 863–881.

Uppala SM, Kallberg PW, Simmons AJ, Andrae U, Bechtold VD, Fiorino M, Gibson JK, Haseler J, Hernandez A, Kelly GA, Li X, Onogi K, Saarinen S, Sokka N, Allan RP, Andersson E, Arpe K, Balmaseda MA, Beljaars ACM, Van De Berg L, Bidlot J, Bormann N, Caires S, Chevallier F, Dethof A, Dragosavac M, Fisher M, Fuentes M, Hagemann S, Hólm E, Hoskins BJ, Isaksen L, Janssen PAEM, Jenne R, Mcnally AP, Mahfouf J-F, Morcrette J-J, Rayner NA, Saunders RW, Simon P, Sterl A, Trenberth KE, Untch A, Vasiljevic D, Viterbo P, Woollen J. 2005. The ERA-40 re-analysis. *Quarterly Journal of the Royal Meteorological Society* **131**: 2961–3012.

Waugh DW. 2005. Impact of potential vorticity intrusions on subtropical upper tropospheric humidity. *Journal of Geophysical Research-Atmospheres* **110**: D11305. DOI: 10.1029/2004JD005664.

Wernli H, Sprenger M. 2007. Identification and ERA-15 climatology of potential vorticity streamers and cutoffs near the extratropical tropopause. *Journal of the Atmospheric Sciences* **64**: 1569–1586.

